The Results of Pulse-Scaling Experiments on Rapid-Growth DKDP Triplers using the Optical Sciences Laser at 351 nm

M. Runkel, A. K. Burnham, D. Milam, W. Sell, M. Feit, A. Rubenchik

U.S. Department of Energy

Lawrence
Livermore
National
Laboratory

December 11, 2000

This report has been reproduced directly from the best available copy.

Available electronically at http://www.doc.gov/bridge

Available for a processing fee to U.S. Department of Energy
And its contractors in paper from
U.S. Department of Energy
Office of Scientific and Technical Information
P.O. Box 62
Oak Ridge, TN 37831-0062
Telephone: (865) 576-8401
Facsimile: (865) 576-5728
E-mail: reports@adonis.osti.gov

Available for the sale to the public from
U.S. Department of Commerce
National Technical Information Service
5285 Port Royal Road
Springfield, VA 22161
Telephone: (800) 553-6847
Facsimile: (703) 605-6900
E-mail: orders@ntis.fedworld.gov
Online ordering: http://www.ntis.gov/ordering.htm

OR

Lawrence Livermore National Laboratory
Technical Information Department's Digital Library
http://www.llnl.gov/tid/Library.html

The results of pulse-scaling experiments on rapid-growth DKDP triplers using the Optical Sciences Laser at 351 nm

Mike Runkel*, Alan K. Burnham, David Milam, Walter Sell, Mike Feit and Alexander Rubenchik

Lawrence Livermore National Laboratory, Livermore, CA 94550

ABSTRACT

Results are reported from recently performed bulk-damage, pulse-scaling experiments on DKDP tripler samples taken from NIF-size, rapid-growth boule BD7. The tests were performed on LLNL's Optical Sciences Laser. A matrix of samples was exposed to single shots at 351 nm (3ω) with average fluences from 4 to 8 J/cm^2 for pulse durations of 1, 3 and 10 ns. The damage sites were scatter-mapped after testing to determine the damage evolution as a function of local beam fluence. The average bulk damage microcavity (pinpoint) density varied nearly linearly with fluence with peak values of approximately 16,000 pp/mm^3 at 1 ns, 10,000 pp/mm^3 at 3 ns and 400 pp/mm^3 at 10 ns for fluences in the 8-10 J/cm^2 range. The average size of a pinpoint was 10(+14,-9) μm at 1 ns, 37±20 μm at 3 ns and ~110 μm at 10 ns, although all pulse durations produced pinpoints with a wide distribution of sizes. Analysis of the pinpoint density data yielded pulse-scaling behavior of $t^{0.35}$.

Significant planar cracking around the pinpoint as was observed for the 10 ns case but not for the 1 and 3 ns pulses. Crack formation around pinpoints has also been observed frequently for Zeus ADT tests at ~8 ns. The high pinpoint densities also lead to significant eruption of near-surface bulk damage. Measurements of the damage site area for surface and bulk gave ratios (A_{surf}/A_{bulk}) of 2:1 at 1 ns, 7:1 at 3 ns and 110:1 at 10 ns.

Maximum aperture averaged transmission losses on the order 15 percent have been measured by photometry for the worst damage at 1 and 3 ns for beam fluences in the 8-10 J/cm^2 range. Analysis of this data yielded a pulse-scaling behavior of $t^{0.25}$ for the obscured area. It was also determined that the crystals used in this test would survive unconditioned exposure to 4 J/cm^2 shots on the NIF laser and still meet the obscuration requirement of 0.1%.

Keywords: KDP, DKDP, bulk laser damage, pulse scaling, frequency conversion, obscuration

1. INTRODUCTION

The goal of these experiments was to determine the pulse-scaling behavior of bulk damage evolution in DKDP. Knowledge of the pulse scaling law is essential for understanding test results obtained from various laser facilities at Lawrence Livermore National Laboratory (LLNL) and applying these results to predict optical performance on the National Ignition Facility (NIF).

Over the course of fusion laser development at LLNL, hundreds of damage tests on KDP and DKDP have been performed using a wide variety of wavelengths and pulse durations. However, deducing a pulse-scaling law from this data[1] has proven to be difficult because of the widely variable nature of crystal quality and the uncertainties associated with the older test methods[2]. Rainer et al[1]. reduced this massive amount of test data and concluded that the KDP/DKDP bulk pulse scaling law followed $t^{0.5\pm0.4}$, which is the behavior (sans error bars) predicted by one dimensional absorptive particle/thermal diffusion damage models. Since then, $t^{0.5}$ scaling has been used to predict damage thresholds at the desired 3 ns pulse duration when test results have become available from damage systems with pulses ranging from 7 to 12 ns.

The shift from measuring damage thresholds to measuring statistical damage distributions with automated test systems has revealed that individual damage events can occur over a wide range of fluences in a given crystal. In addition, recent small-beam, automated damage tests (ADT) have shown a consistent difference in the damage performance of tripler vs. z-cuts for both KDP and DKDP whether rapidly or conventionally grown. Finally, large beam experiments on LLNL's OSL[3] and Slab Lab lasers have shown that the damage "pinpoint" (or micro-cavity) number densities increase steeply with increasing fluence. For example, at a particular fluence the pinpoint density can vary by two orders of magnitude. These results inspired a reinvestigation of the $t^{0.5}$ pulse scaling law used to date.

2. Samples

The samples selected for these tests came from the 50-cm class, rapid growth boule known as BD-7. A large number of tripler samples were cut from this boule for coating development and surface damage testing based on initial test data on z-plates. As shown in Figure 1a, the test results were quite promising with unconditioned (S/1) curves at the NIF damage specification and conditioned (R/1) curves well in excess of it. Subsequent damage tests on tripler samples from this boule showed a substantial drop in performance (see Figure 1b) and led to extensive investigation of the damage differences between tripler and z-plates[4]. The cause of this difference is still unknown, but this effect excluded the BD-7 triplers from being used in surface damage experiments that require high intrinsic bulk thresholds. At the time, BD-7 was considered to be representative of the type of material to be used in early phases of NIF operation, and because of the availability of numerous tripler-cut samples, we decided to use them to study bulk damage pulse-scaling. Prior to the tripler pulse scaling campaign, however, we shot two z-plates and two triplers under nominally identical exposure conditions of 10 ns and ~9 J/cm2 to show that the THG vs. z effect was not an artifact of the Zeus ADT system4. We observed that pinpoint densities for the z-plates were much lower than for the triplers as expected, but these samples have not yet been analyzed for pinpoint density evolution in the manner described below in Section 3.2.
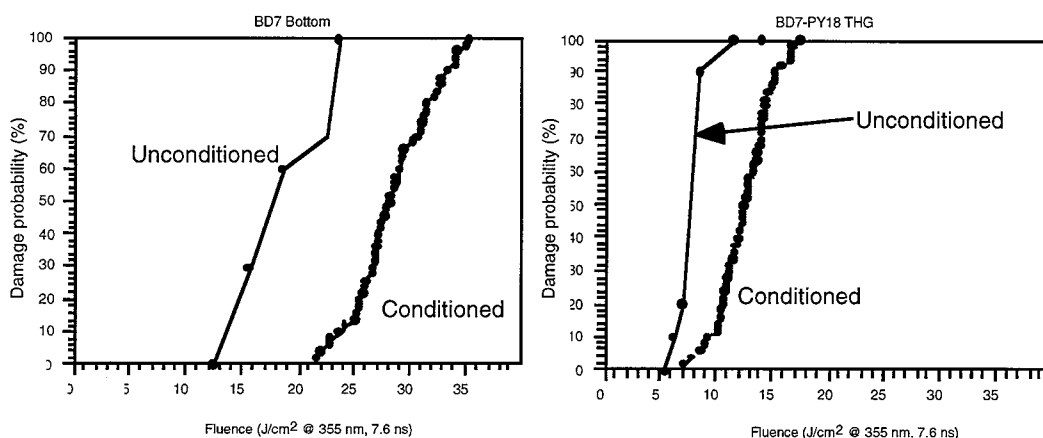

Figure 1. Differences in damage performance between z-plate and tripler samples from rapid growth boule BD-7.

A test plan using six samples was created to study pulse scaling. It called for exposing two samples each at pulse lengths of 1, 3 and 10 ns. Each of the 5-7 test sites per sample was shot with a single pulse (1/1) of 351-nm light. Average beam fluences ranged from 4 to 10 J/cm2. The typical level of fluence modulation in the ~1 cm diameter beam was 1.3:1 (peak:average). The tests were performed in a vacuum of ~ 10-5 to 10-6 Torr, and beam energy, temporal and spatial profiles were recorded for each shot. A Schlieren scatter imaging system was also used to record damage at each site during the test, but this data was not used for analysis. The experimental layout is shown in Figure 2.
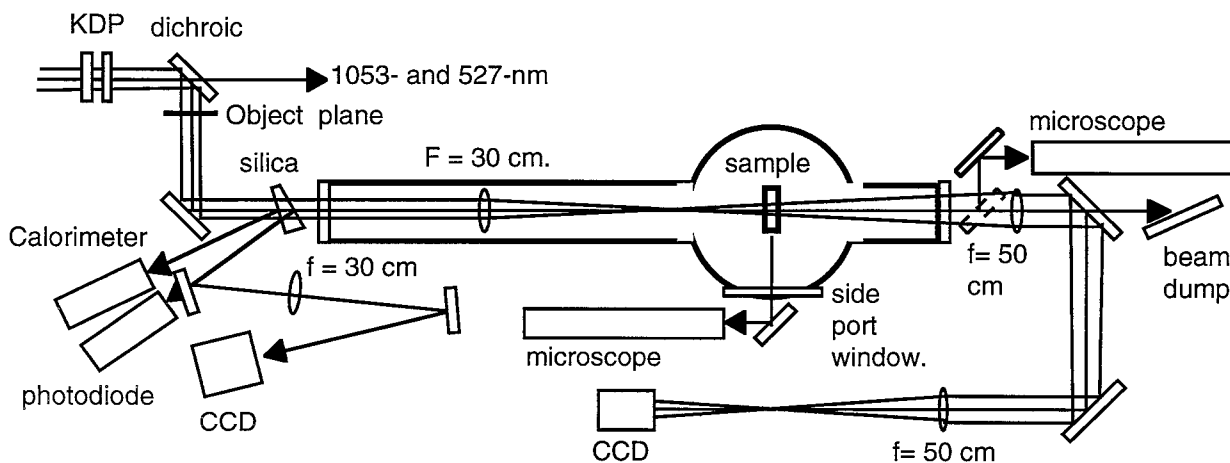

Figure 2. Schematic of the OSL t-scaling experimental layout. The output plane of the OSL conversion crystals was imaged on the damage test samples. Vacuum was required to prevent air breakdown at the 30-cm lens focus.

3. Post test analysis

After laser exposure in OSL, sites were analyzed on the following three samples: BD-7-PY-37 (1 ns), BD-7-PY-27 (3 ns) and BD-7-4 (10 ns). The analysis consisted of microscopic inspection using Nomarski and darkfield microscopy up to 200X magnification followed by scatter mapping. For the microscopic inspections two microscopes were used. First, samples were characterized using a Navitar zoom microscope looking into the sample at 90 degrees from the beam propagation direction. Illumination for the images taken with this system was provided by a HeNe beam of 150-_m 1/e2 diameter. This setup was also used to calibrate pinpoint density to scatter signal as described in section 3.2 and Appendix 1. After this, an Olympus microscope was used to inspect sample along the beam propagation direction or THG axis. The results of these inspections are given in sections 3.1.

3.1 Post-exposure microscopic inspection

Microscopic inspection of the samples after testing immediately revealed substantial differences in pinpoint density and size between the three pulse durations. We observed that the shorter pulse lengths generated smaller pinpoints at significantly higher densities for a given fluence level. Figure 3 shows damage tracks taken with the side-looking Navitar microscope. The depth of focus of the image is approximately 100 μm and the spatial resolution limit is approximately 5 μm.
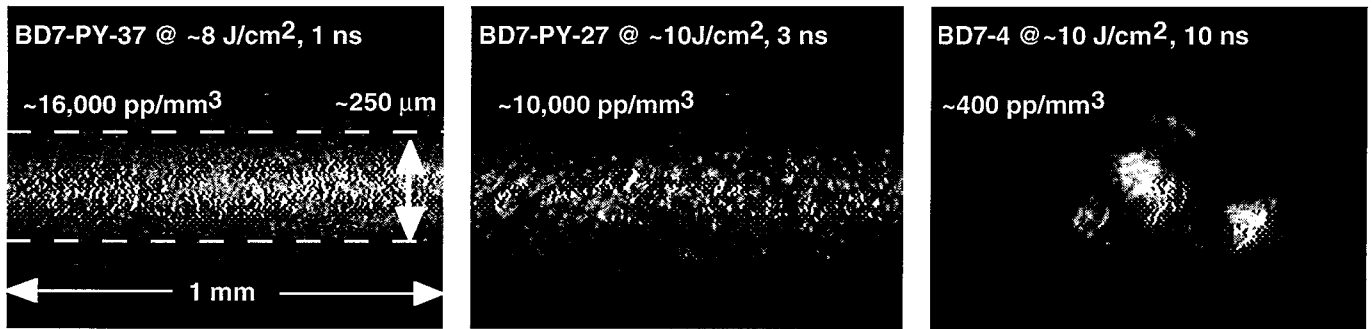

Figure 3. Damage track images from the side-looking Navitar microscope showing the differences in pinpoint density and size for 1, 3 and 10 ns pulses in the 8-10 J/cm^2 fluence range. The irradiated region is approximately 250 μm in diameter. These are the highest pinpoint densities measured for each pulse duration.

Pinpoint densities given in the Figure 4 were obtained by thresholding the image then using particle counting and sizing algorithms in the *NIH Image* program. The number density in the irradiated volume was then determined using the 150-μm HeNe diameter. No attempts were made to account for differences in illumination due to the gaussian profile of the HeNe or for obscuration of back pinpoints by ones in front. When the samples were scatter mapped, the high density of pinpoints in the 1 and 3 ns cases caused the PMT to act nonlinearly (see Appendix1). The images shown in Figure 3 represent the highest pinpoint densities measured for their respective pulse durations in the 8-10 J/cm^2 range. For 1 ns, this value was approximately 16,000 pinpoints per mm^3 while for 3 and 10 ns the densities were ~10,000 pp/mm^3 and ~400 pp/mm^3 respectively. At the ~100X magnification, the damage track images of the 1 and 3 ns samples show little structure. This is in marked contrast to the 10-ns case where the damage microcavity is much larger and shows crack propagation away from the central cavity. Microcavity size distributions determined from these images are shown in Figure 4. As indicated in Figures 3 and 4, the 10-ns sites are much larger. The observed size is due to the HeNe beam being reflected off crack surfaces that extend two to three times beyond the radius of the central microcavity. The situation is different for shorter pulse lengths. The 1- and 3-ns distributions of Figure 4b indicate that the shorter pulse has a higher percentage of smaller (~5 μm length) microcavities. This changes for sizes greater than about 8 μm where the 3-ns distribution then has a higher percentage of total sites than at 1 ns.
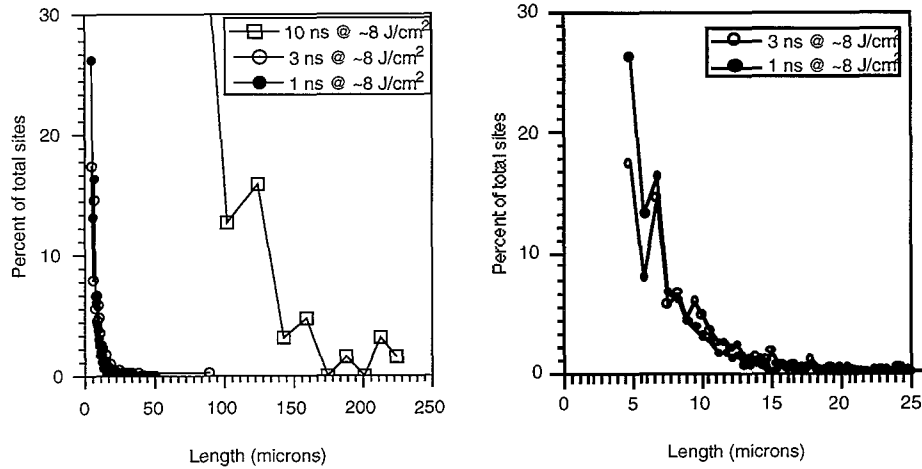
Figure 4. Size distributions for 1, 3 and 10 ns damage track images. Figure 6b shows only the 1 and 3 ns distributions on an expanded length scale. The 1 ns data shows a higher percentage of 5 micron damage sites but the 3 ns data has a higher percentage of larger sites.

When the data of Figure 4 are plotted on a log-log plot, they appear linear with the exponent (slope) approximately equal to -3 (see Figure 5 below).
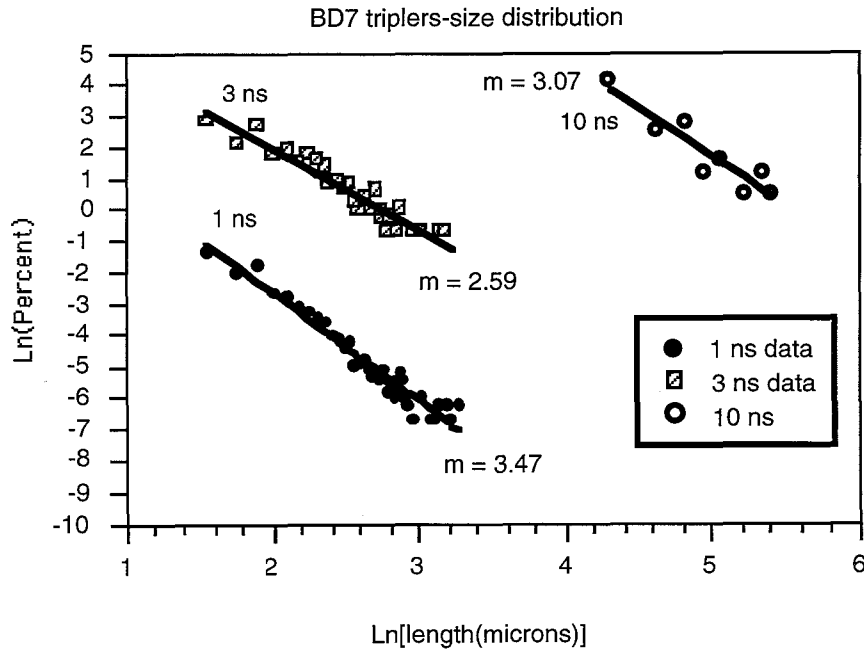

Figure 5. Log-log plot of pinpoint sized distribution data from Figure 4 of the main text. The power law exponents for each pulse duration all are near m=3.

The fit parameters for the 1 ns data are m=3.47 and A=4.3 where the fit equation is ln(%)=ln(A)-mln(l). For the 3 ns data, the fit parameters are m=2.59 and A=7.1, and for 10 ns m=3.07 and A=17.1. It is interesting that the power law exponents for each pulse duration are near m=3. This consistent behavior between pulse durations is compelling and we are currently developing a power law model[9,10] to account for it. In its current form, the power law model predicts that pinpoint density evolves according to –6th power of the size, however, this behavior must be reconciled with the apparent linear evolution of pinpoint density with fluence described in section 3.2 below.

Additional microscopic inspection at 200X confirmed the variation in size and number density over the pulse length range. The images of Figure 5 are from looking along the tripler axis as opposed to 90° to it. At 200X, no crack formation was

observable for the 1-ns damage microcavities. For the 3-ns microcavities, crack formation was quite rare, while at 10 ns, the microcavities were almost always accompanied by cracks. Analysis of the Figure 6 images also showed the increase in size of the pinpoints with pulse duration. At 1 ns the average length (Area$^{0.5}$) was 3.5±3.8 μm, while for 3 and 10 ns it was 7.1±7 μm and 28 μm respectively. Again, the 10 ns pinpoint is substantially larger, following the general trend found for the side-looking images. At this time, we believe that the size differences observed between the two views are real and reflect the difference between the central damage core and the extended fractures visible in the side projection. It is also interesting to note that the measured lengths scale roughly as the pulse duration. The ratio of average lengths from 3 to 1 ns is 7.1/3.5 = 2.0, while between 10 and 3 ns it is 28/7.1 = 3.9. If the plasma generated by the initial damage event is supported by additional laser energy in the pulse (e.g. the laser-supported detonation wave), this behavior is expected.
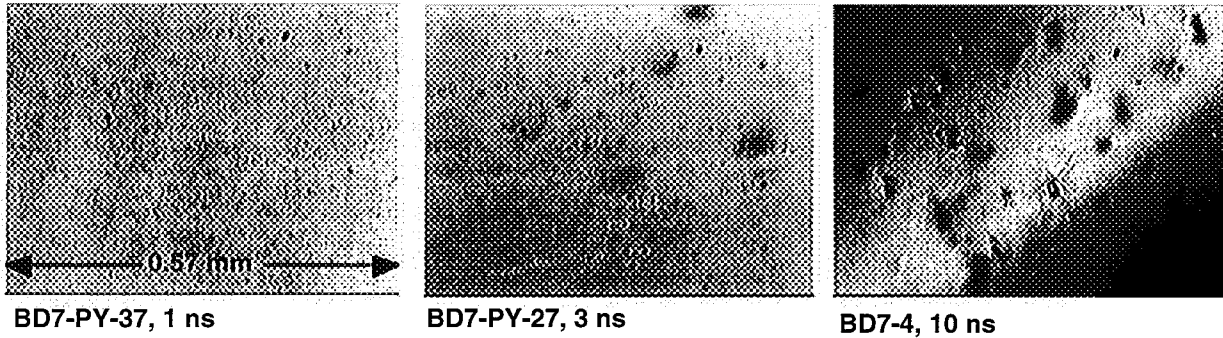

BD7-PY-37, 1 ns **BD7-PY-27, 3 ns** **BD7-4, 10 ns**

Figure 6: Bulk damage viewed along the direction of beam propagation for 1, 3 and 10 ns cases at ~8-10 J/cm^2. Cracks at the damage sites rarely occur for 1 and 3 ns, but are frequent at 10 ns.

Surface damage due to eruptions of bulk pinpoints was also noted for the peak pinpoint densities at all three pulse lengths. Examples are shown in Figure 7. Image analysis of the surface damage sites made it possible to determine the ratio of surface to bulk damage area (A_{surf}/A_{bulk}), which increased from 2.4 at 1 ns to 6.9 and 109 at 3 and 10 ns, respectively. These results are tabulated in Table 1.

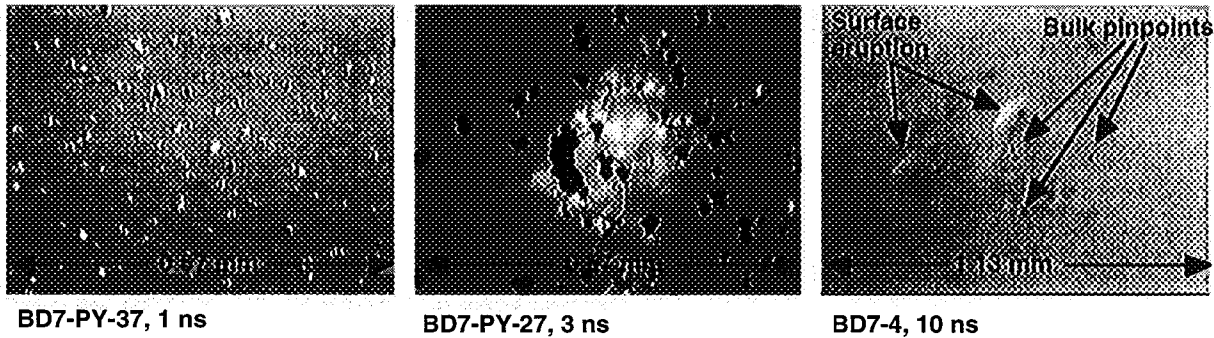**BD7-PY-37, 1 ns** **BD7-PY-27, 3 ns** **BD7-4, 10 ns**

Figure 7. Damage cause by eruption of near surface bulk pinpoints. The ratio of surface to bulk area increases at longer pulse lengths.

Table 1. Results of microscopic investigation of BD-7 tripler test sites. The length is simply $A^{0.5}$.

Measurement	1 ns	3 ns	10 ns
Max. pinpoint density	~16,000 pp/mm^3	~10,000 pp/mm^3	~400 pp/mm^3
Average area (90° view)	0.0001±0.0002 mm^2	0.0014±0.0004 mm^2	0.0125 mm^2
Average length (90° view)	10±14 μm	37±20 μm	111μm
Average area (THG axis)	1.25±1.42x10^{-5} mm^2	5.1±5.0x10^{-5} mm^2	8x10^{-4} mm^2
Average length (THG axis)	3.5±3.8 μm	7.1±7 μm	28.8 μm
Average area (THG surface)	3.0x10^{-5} mm^2	3.5x10^{-4} mm^2	0.0086 mm^2
Average length (THG surface)	5.4 μm	18.7 μm	93 μm
A_{surf}/A_{bulk} (THG axis)	2.4	6.9	109

2.2 Scatter mapping of damage sites

In order to correlate the damage pinpoint density with local beam fluence, the spatial profiles were converted to fluence maps taking beam energy, camera pixel counts and system magnification into account. Next the samples were scatter mapped on the Zeus ADT system with spatial resolution comparable to the OSL beam profiles. As shown in Figure 8, the samples were scatter mapped by stepping them across a HeNe laser that was focused to a beam diameter of 150 µm (FW@1/e^2). The scattered HeNe light was imaged onto a photomultiplier tube and the voltage output from the PMT was recorded by computer during the scanning process. The scatter diagnostic was calibrated to pinpoint density by imaging the scatter track from the side. The number of pinpoints and their size were measured using *NIH Image* software on the electronic images and a calibration curve was built for each sample tested. This voltage to pinpoint density curve was then used to convert the scatter maps to pinpoint density maps.
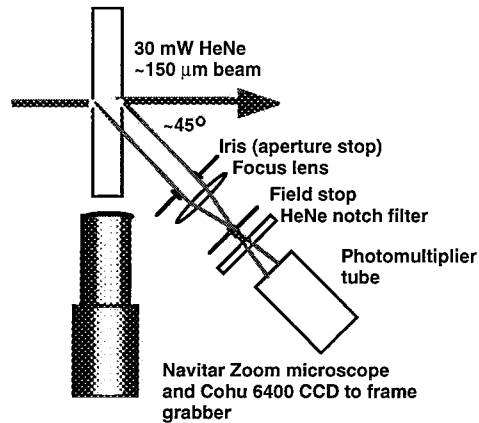

Figure 8. Schematic of the diagnostics used to scatter map damage sites and calibrate PMT voltage to pinpoint density.

Once the pinpoint density maps were produced they were compared to the fluence profiles. This was done by taking horizontal and vertical cross-sections through common features in each map. The scales of the fluence and pinpoint density lineouts were adjusted to provide the best match of features, then the pinpoint density lineout was interpolated to provide a direct "cell-by-cell" comparison to the local fluence lineout. The process is shown in Figure 9 and was used in previous OSL work[3].
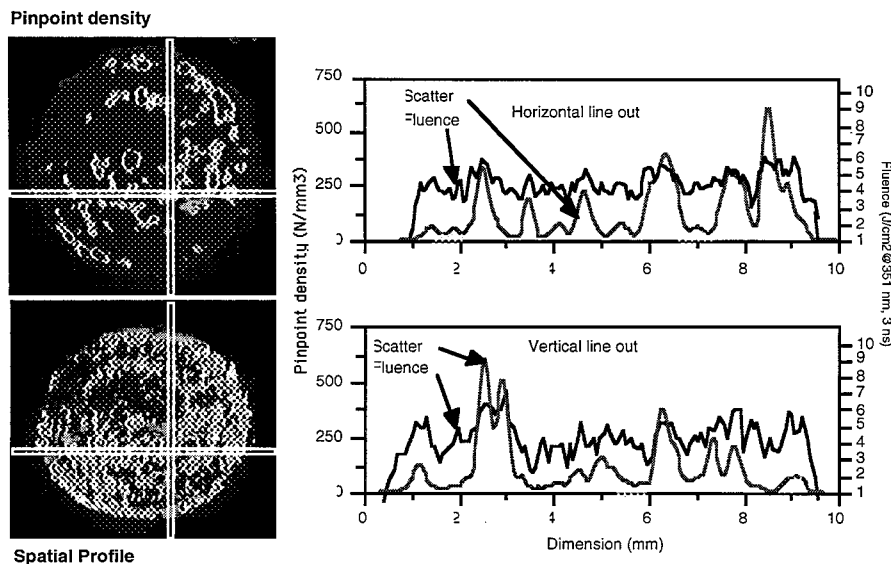

Figure 9. Comparison of pinpoint density map to spatial fluence profile. Horizontal and vertical lineouts were taken from each map then scaled and interpolated to provide cell-by-cell comparison of pinpoint density to local beam fluence.

At this stage the pinpoint density was plotted against the fluence to show the damage evolution. Figure 10a shows the pinpoint density obtained from scatter mapping plotted against the local beam fluence, while Figure 10b shows the data plotted as a function of local irradiance. The data shows essentially linear evolution in pinpoint density for all the pulse durations. At 1 and 3 ns the curves are a combination of lineout data from two different test sites, one being the site exposed to the highest average fluence, and the other a site of approximately half the maximum average fluence. This was initially done to determine whether the damage evolved along the same curve different average fluence levels. When this was confirmed, both sites were combined into the data sets shown in the figure.

The linear pinpoint evolution was unexpected based on the exponential evolution results obtained for the OSL conditioning campaign[3]. The differences are attributable to changes in the method of calibrating the photomultiplier tube between the two campaigns, and we consider the data presented here to be most representative of pinpoint evolution. The calibration methods are discussed in detail in Appendix A.
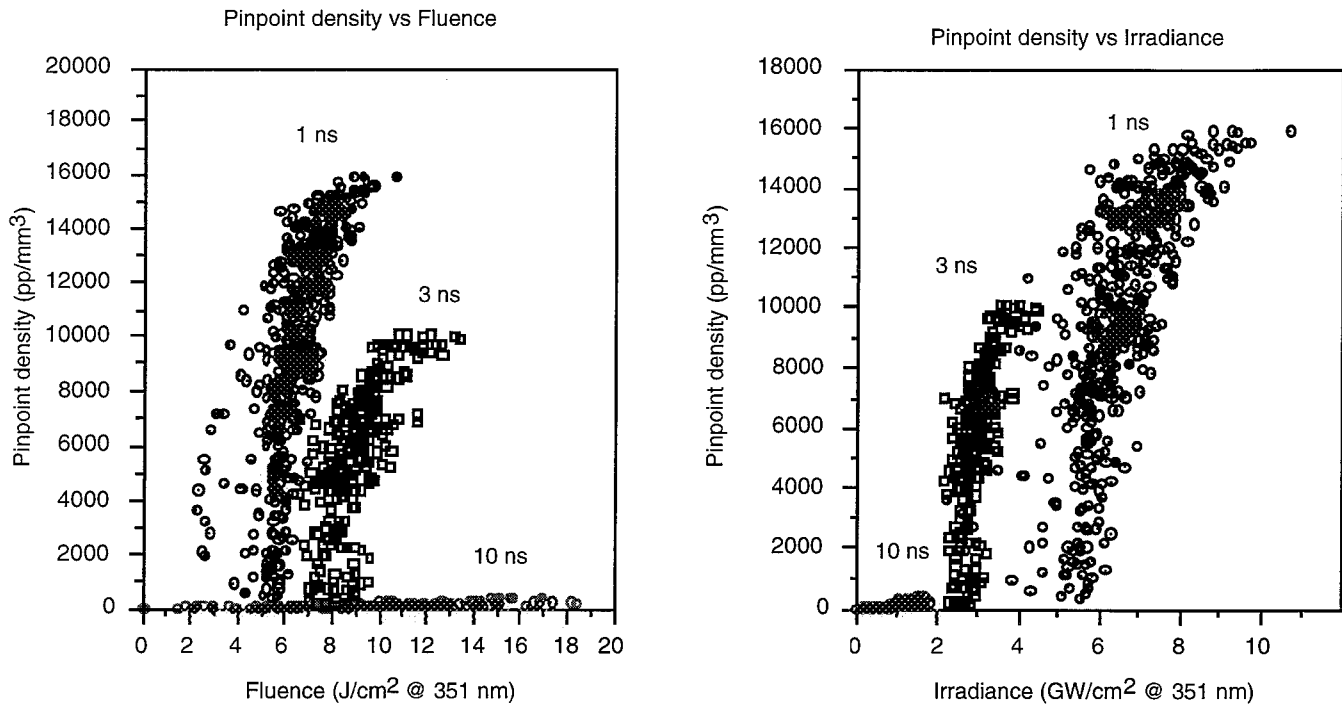

Figure 10. Pinpoint density evolution with different pulse duration as a function of local beam fluence for BD-7 triplers.

2.3 Pulse scaling

In order to investigate the pulse-scaling behavior of the data, the procedure given by Feit et al. was followed. In their paper[6] discussing the heating of small absorbing particle by linear absorption, these authors showed that from heat diffusion arguments, one can expect the temperature at/near an absorbing inclusion to follow a $F/t^{0.5}$ dependence *or less*, where F is the beam fluence. Assuming that the damage threshold is related to a critical temperature, the damage pulse scaling should also follow this dependence. To examine this, Feit et al. took the data of Figure 10 and normalized the pinpoint density. Next they scaled for pulse duration by dividing the fluence by $t^{0.5}$. This made the data overlap quite well. We repeated their analysis but allowed the fluence to be scaled as t^n where n could be any number. The highest degree of overlap was obtained with n=0.35. This is shown in Figure 11 and represents the first set of experimental data that indicate the pulse scaling for DKDP deviates from $t^{0.5}$.
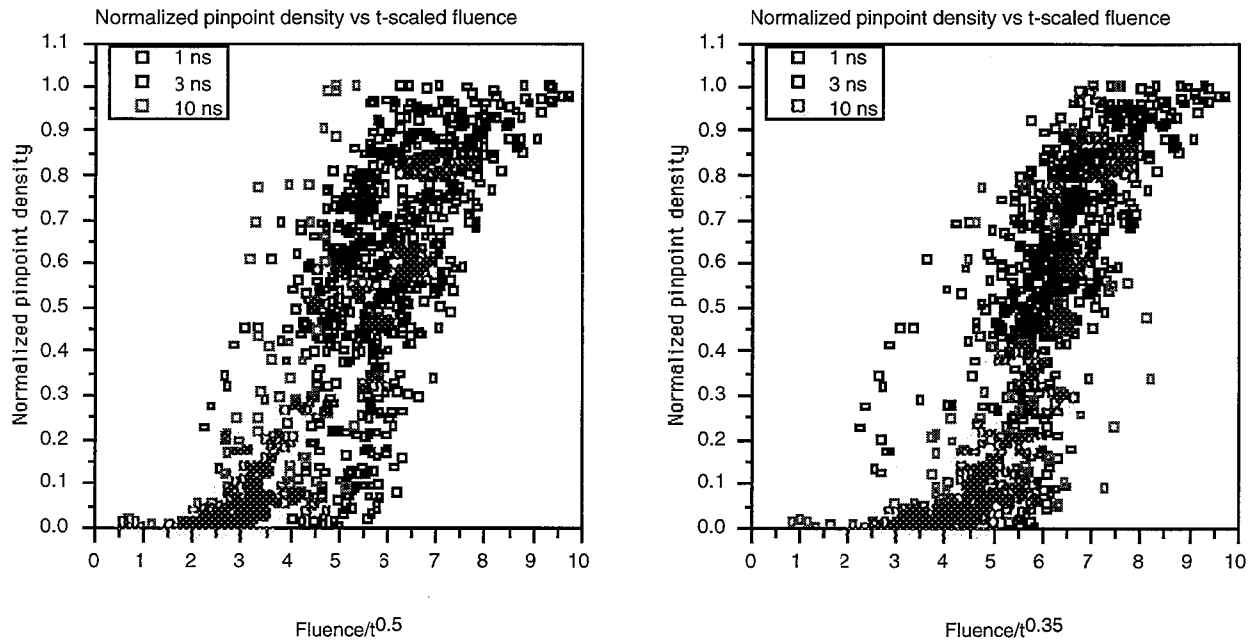
Figure 11. Normalized and temporally scaled pinpoint densities for BD-7 triplers at 1, 3 and 10 ns. Figure 11a shows the $t^{0.5}$ scaling while Figure 11b shows $t^{0.35}$ scaling.

2.4 Scatter loss and obscuration

With pinpoint densities on the order of 10,000 per mm^3 the 1 and 3 ns damage sites appear milky white when viewed by eye (see Figure 12). This indicates high scattering losses.
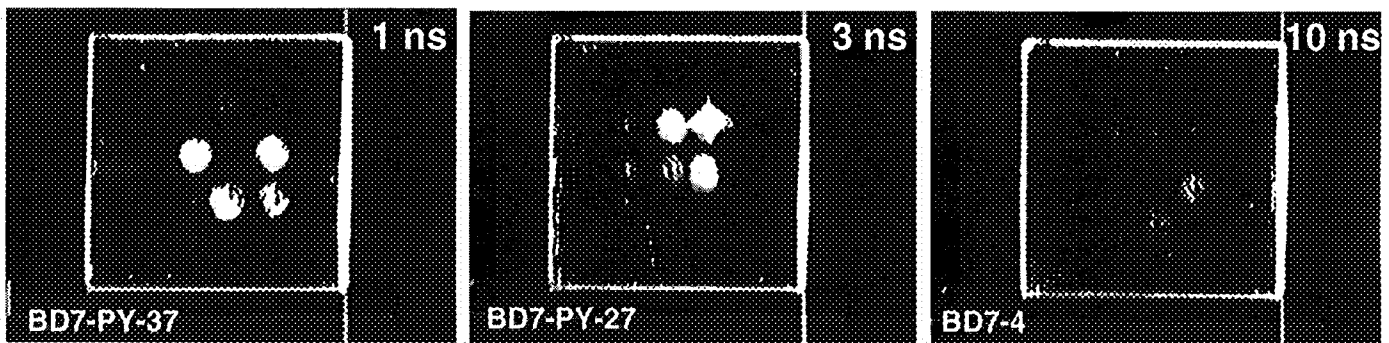
Figure 12. Darkfield images of the BD-7 samples showing the degree of white light scatter from damage sites.

To determine how large scattering was, we measured obscuration losses by 3ω photometry scans as shown in Figure 13, where the image colors were scaled to match visually with the photographs of Figure 12. As expected, the measurements show that the transmission drops significantly for the higher fluence shots. The acceptance angle (field of view) of the photometer for these measurements was on the order of 1-3 mrad. These results are also shown in Table 2.

Figure 13. Photometry scans at 3ω on BD-7 damage samples. Site numbers are given for comparison to transmission loss in Table 2. Only the very low fluence sites at 1 and 3 ns pulse lengths would pass the NIF loss specification of 0.1%. Black color in all the images indicates transmission below 88%. The large site next to 2005 for the 3 ns case resulted from multiple shots and was not considered in the analysis.

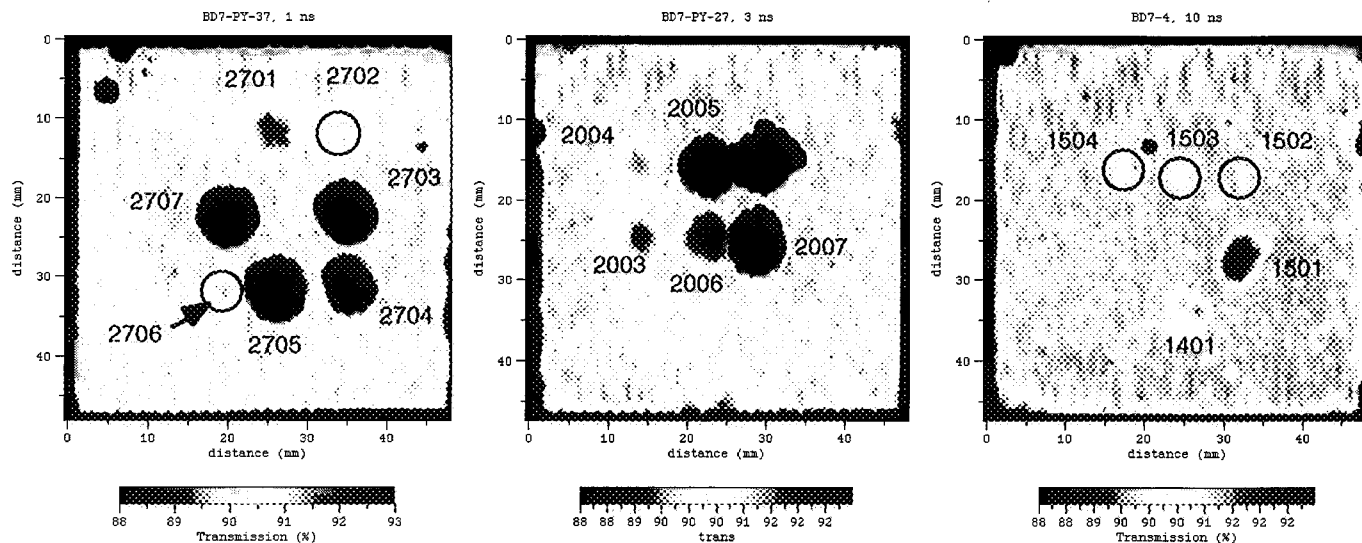Table 2. Average transmission versus average beam fluence. Fresnel surface losses have been accounted for in the data.

Sample	Site number	Average fluence (J/cm^2)	Average Irradiance (GW/cm^2)	T_{photom}(%)
BD-7-PY-37	2701	4.3±1.1	4.3±1.1	99.2
(1 ns)	2702	4.1±0.9	4.1±0.9	99.6
	2703	6.3±1.6	6.3±1.6	89.5
	2704	5.1±1.8	5.1±1.8	95.4
	2705	5.9±2.0	5.9±2.0	87.2
	2706	3.8±1.1	3.8±1.1	99.5
	2707	6.1±1.5	6.1±1.5	88.3
BD-7-PY-27	2003	5.6±1.4	1.9±0.5	99.1
(3 ns)	2004	5.7±1.6	1.9±0.5	99.4
	2005	7.5±2.5	2.5±0.8	85.8
	2006	6.7±2.0	2.2±0.7	97.7
	2007	7.8±1.8	2.6±0.6	83.6
BD-7-4	1401	7.5±2.2	0.8±0.2	99.4
(10ns)	1501	9.1±2.2	0.9±0.2	98.1
	1503	6.5±1.6	0.7±0.2	99.9
	1504	6.3±1.8	0.6±0.2	99.9
	1505	3.6±1.2	0.4±0.1	99.9

Transmission vs fluence

(plot with legend: 10ns ●, 3ns ■, 1ns ○; axes Transmission (%) vs Fluence (J/cm2 @ 351 nm); labels "10 ns", "1 ns", "3 ns")

Transmission vs irradiance

(plot with legend: 10ns ●, 3ns ■, 1ns ○; axes Transmission (%) vs Irradiance (GW/cm2 @ 351 nm); labels "10 ns", "3 ns", "1 ns")
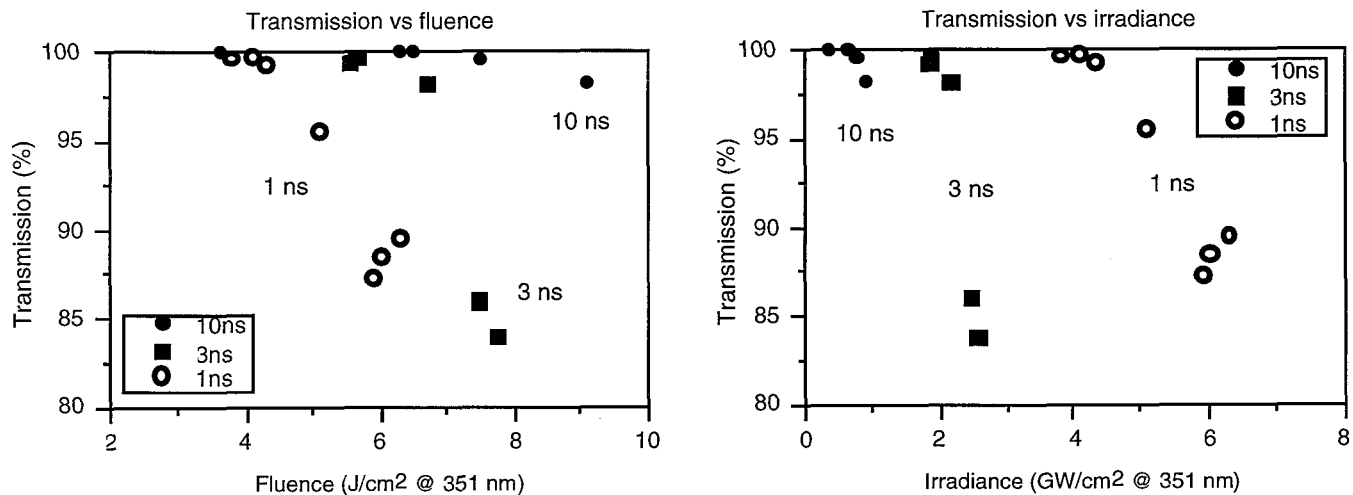
Figure 14. Plots of transmission versus beam fluence and irradiance. The data show significant transmission loss at fluences near the NIF full fluence average (8 J/cm^2 at 3 ns). The transmission loss is worse for the 3 ns case.

Figure 14 shows the photometry data plotted as a function of average beam fluence and irradiance. The transmission loss is significant (>10%) for all pulse durations at fluences greater than about 6 J/cm^2. The data shown in Table 2 have been adjusted to take Fresnel surface losses into account. The 10-ns shots result in the lowest amount of transmission loss (1.9% at ~ 6 J/cm^2) despite having substantially larger obscuration/site. At the other pulse extreme, the 1-ns data starts to show substantial loss at fluences above 4 J/cm^2 (GW/cm^2) and reaches a maximum loss of 12.8% at 6 J/cm^2 (GW/cm^2). The 3 ns case gives the maximum amount of loss which becomes substantial starting at fluences exceeding 6 J/cm^2 (2 GW/cm^2).

Figure 15 shows the results of pulse scaling the photometry transmission data using t^n scaling in a similar manner to the pinpoint density data. The best overlap of the photometry transmission curves is obtained with n=0.25. The data is also plotted as a function of obscuration, i.e. 100-Transmission(%), and was found to follow an exponential form quite well.

Transmission vs scaled fluence

(plot with legend: T10ns ●, T3ns ⊡, T1ns ○; axes Transmission (%) vs Scaled fluence [F*(3/t)$^{0.25}$])

Obscuration vs scaled fluence

(plot with legend: T10ns ●, T3ns ⊡, T1ns ○; axes Obscuration (%) vs Scaled fluence [F*(3/t)$^{0.25}$]; equation and NIF spec line)
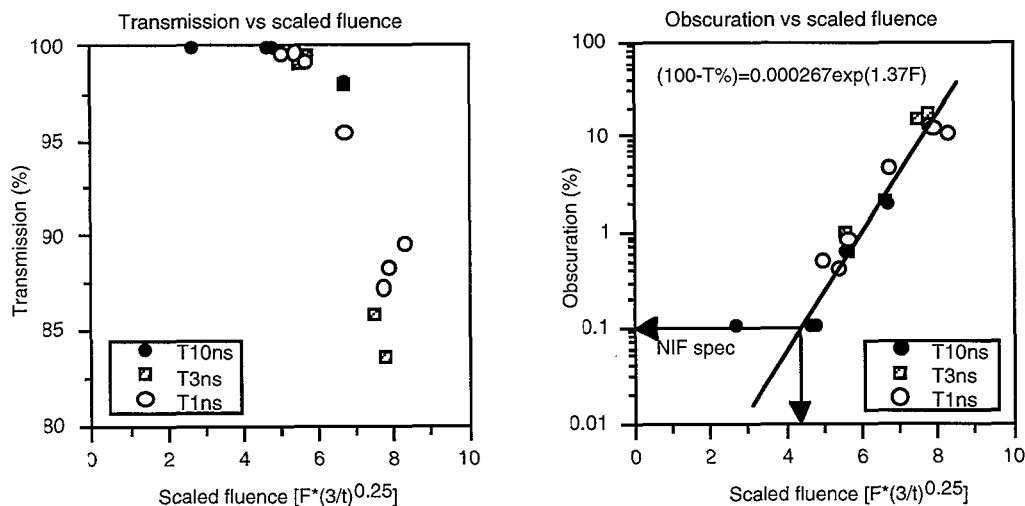
(100-T%)=0.000267exp(1.37F)

NIF spec

Figure 15. Results of t^n pulse scaling on photometry data. The best overlap in the scaled data is with a value of n=0.25. The data exhibits exponential behavior and indicates that BD-7 material could survive 4 J/cm^2 shots without conditioning.

4.0 DISCUSSION

The change in pinpoint density, size distributions, and obscuration with pulse duration had not been previously quantified. These results will have a substantial impact on our implementation of future tests and interpretation of data to predict NIF crystal performance.

4.1 Pulse scaling

The overlap scaling method applied to the normalized pinpoint density data of Figures 9 and 10 indicates that $t^{0.35}$ scaling gives the best overall match between the data. As noted earlier this is the first definitive indication that DKDP does not follow the $t^{0.5}$-scaling rule. This is not entirely unexpected, as many optical materials do not follow $t^{0.5}$ scaling[1]. In addition, the obscuration measurements show a scaling exponent of 0.25. Before adopting 0.3 as the new (general purpose) scaling exponent, critical examination of these experiments is in order. First, the samples used in these tests are not currently regarded as the best quality producible by rapid-growth methods. Additional, better, samples would also have to show the $t^{0.3}$ scaling, and these samples typically show a markedly lower pinpoint density at these fluences. Second, the high pinpoint densities produced in the 8-10 J/cm^2 range were somewhat unexpected. While our measurements show that the material could survive unconditioned shots of 4 J/cm^2, it is clear that this material would never be installed on the NIF without some form of laser preconditioning. It is therefore imperative to test the effect of laser conditioning on damage evolution and pulse scaling. The 1997 OSL laser conditioning campaign[3] was our first attempt at this and showed significant laser conditioning with just a few low fluence shots. However, the only samples tested were z-plates, which we now know have significantly different damage properties than triplers. The pulse-scaling law may change according to the quality of crystal, its cut and the degree of laser conditioning.

Several reports and publications discuss the subject of pulse scaling at some length[7-9]. All of these works have started out with a one-dimensional diffusive heat flow model from which the $t^{0.5}$ scaling occurs naturally. Deviations from the square root law are required to be inserted into the theoretical formalisms "by hand", and a number of mechanisms have been proposed to account for them. Despite this, these theories give pulse-scaling behaviors close to the non-square-root scaling observed for many different optical materials. However, no models currently exist to address the phenomenon of laser conditioning and its effect on damage evolution.

4.2 Obscuration and scatter losses

The photometry measurements presented above indicate that it is quite easy to exceed the NIF loss specification for triplers (0.1%) in a moderate fluence situation if the crystals are not preconditioned in some manner. The effect of laser conditioning can be seen in Figure 16 which shows the transmission loss measured by photometry and the damage probability associated with the BD-7 triplers.
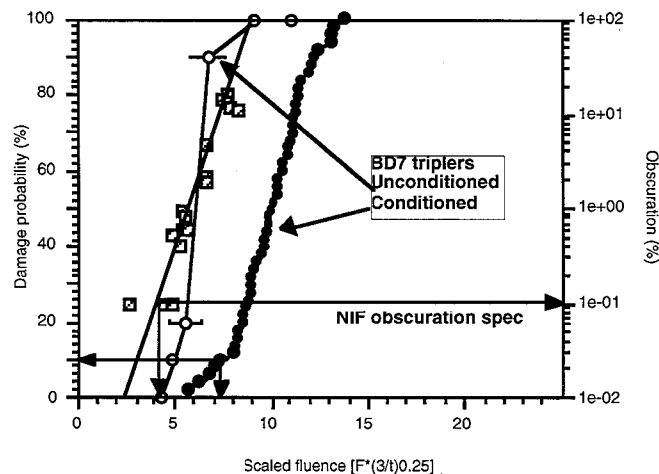

Figure 16. Comparison of BD-7 pulse scaled photometry obscuration and Zeus ADT scaled damage probability measurements. The scaling used was $t^{0.25}$ for both transmission and damage probability data. Comparison of the damage probability curve with the obscuration curve indicates 10% damage probability is similar to the NIF scattering specification.

The NIF specification of 99.9% transmission corresponds approximately to a 3 ns-scaled fluence value of 4.3 J/cm^2 (5.7 J/cm^2 at 7.6 ns of the Zeus ADT) for the S/1 damage data. This corresponds to 10%damage probability when the ±15% fluence measurement error is incorporated in damage probability curves. The data also shows the value of laser conditioning. Scaling the R/1, 10% damage probability fluence gives a fluence of 7.3 J/cm^2 at 3 ns as the maximum fluence a conditioned BD-7 tripler could still meet the obscuration specification. Taking beam modulation into account, a 10 percent damage probability at roughly 10 J/cm^2, 3 ns should provide safe margins for a full fluence shot. The degree of laser conditioning exhibited by BD-7 crystals was slightly lower than average so higher damage resistance can be expected from future crystals.

In the previous OSL conditioning campaign, we deduced that the DKDP11 z-plate sample would just meet the NIF obscuration specification, but this was based on a simple obscuration model where we assumed a fixed damage area of 1 μm^2. Clearly this value was too small, but the exponential evolution used to calculate obscuration may have fortuitously given a reasonable result. The information developed in this report will be used to reassess the validity of our previous conclusion. However, until we have learned to interpret the low-angle scatter measurements, the DKDP11 curve will still be used to guide crystal development.

The standard battery of S/1 and R/1 tests on the Zeus ADT system can still be used to assess progress in crystal R&D. However, a more reliable test for quality assurance purposes would be to raster scan the QA samples with a 3-ns laser by ramping up to the desired operating fluence of 4, 6 or 8 J/cm^2, then measure the actual scatter loss.

ACKNOWLEDGMENTS

REFERENCES

1. F. Rainer, F. De Marco, M. C. Staggs, M. R. Kozlowski, L. J. Atherton, L. M. Sheehan, "A historical perspective on fifteen years of laser damage thresholds at LLNL," SPIE Proceedings, Volume 2114, 9-22, 1993
2. Mike Runkel, "Monte Carlo simulation of the R/1 automated damage test," SPIE Proceedings, Volume 3578, 277-289, 1998
3. Mike Runkel, Jim DeYoreo, Walt Sell and David Milam, "Laser conditioning study of KDP on the Optical Sciences Laser using large area beams," SPIE Proceedings, Volume 3244, 51-63, 1997
4. Mike Runkel and Alan Burnham, "Differences in the damage probability distributions between tripler vs. z-cuts of KDP and DKDP at 355 nm" SPIE Proceedings of this symposium, October 2000
5. Mike Runkel, Alan Burnham, Curt Neeb, Mary Norton and Paul Wegner, "Results of Slab Lab DKDP surface damage growth experiments," NIF-37913, November, 1999
6. Mike Feit, Alexander Rubenchik, Mike Runkel, "Analysis of bulk DKDP damage distribution, obscuration and pulse length dependence," SPIE Proceedings of this Symposium, 2000
7. David Eimerl, "Pulse length scaling of damage thresholds in insulators: Why do they scale as t$^{0.4}$ rather than 0.5 from about 10 ps to 1000ns?" LLNL internal memo, July, 1994
8. John Trenholm, "Damage from pulses with arbitrary temporal shapes," LLNL Internal Memo, LST-LMO 94-001 (Version 2), October, 1995
9. Mike Feit and Alexander Rubenchik, "Pulse shape and pulse length scaling of ns pulse laser damage threshold due to rate limiting thermal conduction," SPIE Proceedings, 3244, 5-11, 1997
10. Mike Feit, Personal communication on the topic of DKDP bulk damage defect distributions from obscuration measurements, 2000
11. Mike Feit, Alexander Rubenchik, Mark Kozlowski, Francois Genin, Sheldon Schwartz, Lynn Sheehan, "Extrapolation of damage test data to predict performance of large-area NIF optics at 355 nm," SPIE Proceedings, Volume 3578, 226-234, 1998

APPENDIX 1.

Calibration of pinpoint density to scatter voltage

A1.1 Introduction

This appendix describes the details of calibrating the photomultiplier tube to convert the measured scatter voltage to pinpoint density. It is included because the measured response was not linear for the 1 and 3 ns cases. We believe this is due to the scatter losses for high densities of pinpoints and is not related to the intrinsic response of the photomultiplier tube itself. The response curve was not measured in this way for the OSL conditioning tests[3] when a simpler, less precise method was employed. That method showed linear PMT response and the lineout analysis led to the conclusion that pinpoint density evolved exponentially. In contrast, the method used here shows that pinpoint density grows in a more linear fashion.

A1.2: PMT calibration method

As described in Section 3.2, the damage sites were scatter mapped using the diagnostic shown in Figure 8. Once mapping was complete, the sample was moved in the HeNe beam to obtain output voltages in approximate 1volt increments ranging from 0-10 Volts. The output of the PMT was limited to 10 volts by a Zener diode to prevent damage to the computer's data acquisition board. Prior to mapping, neutral density filters were used to attenuate the HeNe beam to limit the scatter voltage at the maximum pinpoint density to slightly less than 10 volts. At each point where a calibration voltage was recorded, the Navitar system was used to image the associated pinpoint density. Prior to use, the Navitar system was calibrated to image 1.0 mm along the HeNe axis. To photograph the majority of scatterers, the Navitar was located on a z-axis stage and moved 1.0 mm along the HeNe scatter track for each image. Typically 8-10 images for each scatter track/voltage level were recorded. The frame grabber board in the computer binned the 1.0-mm distance into 320 pixels giving a resolution of 3.1 μm/pixel. The intensity resolution of the camera was 8-bit or 256 gray levels. *NIH Image* software was used to analyze the images. The analysis consisted of subtracting background levels and thresholding the image appropriately to provide a good visual match to the unaltered image. This was a subjective exercise, and the background subtraction and thresholding parameters changed slightly over the course of analysis to provide a balance between losing dim sites and bleeding pixels together for bright sites. The number of sites in each image was recorded and averaged to provide statistics. The pinpoint density was calculated based on the known diameter of the HeNe beam and the thickness of the image (or portion of image) being evaluated. No corrections were made to the pinpoint densities based on the gaussian profile of the HeNe illumination or to account obscuration of rear pinpoint by ones in front. To determine the size distributions for 1 and 3 ns shown in Figure 4, a single image of maximum pinpoint density was evaluated. The software was set to recognize as particles only those features containing more than 2 pixels. This was thought to be a good discriminator between real features and noise as well as those small or poorly illuminated sites that would not contribute significantly to the scatter signal. This accounts for the limit in size of approximately 5 μm on the Figure 4 plots.

After the image analysis, the pinpoint density was plotted as a function of scatter voltage. The results are shown in Figure A1-1.
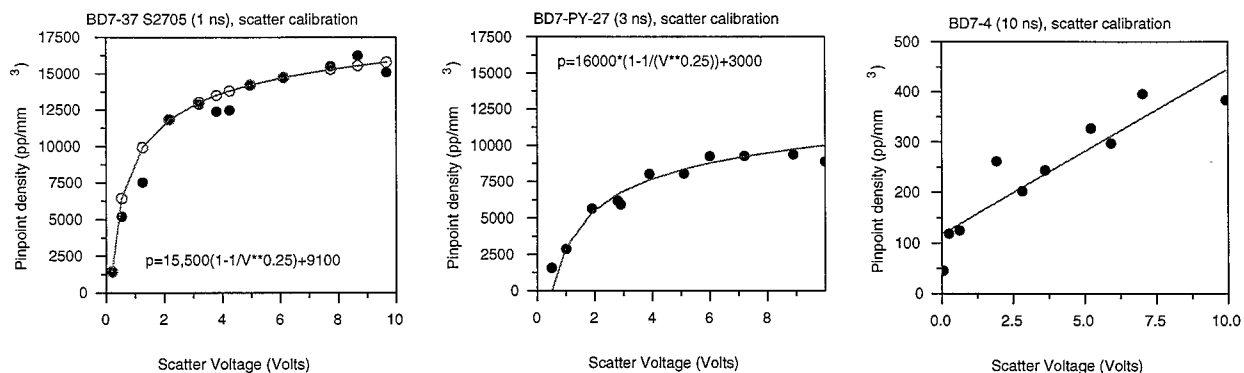

Figure A1-1. Scatter calibration curves for BD-7 triplers exposed to 1, 3 and 10 ns pulses. The 10-ns curve behaves linearly but the 1 and 3 ns curves display significant nonlinearity.

The differences between the 10-ns calibration curve and the 1 and 3 ns data indicate that the PMT's intrinsic response is linear. Consequently, we interpreted the 1 and 3 ns curves to be due to scatter loss by multiple reflections or obscuration.

As a result, it is likely that we have underestimated the number, and overestimated the size, of the scattering distributions; and better measurements will be required to answer these questions.

We devised a fitting function of the form: $\rho=\rho_0(1-1/V^a)+\rho_1$ for the 1 and 3 ns cases. This fit the data reasonably well for parameters indicated in the figure and was then applied to the scatter maps to determine pinpoint density. We did not dwell on determining any physical significance to the fitting function. A comparison between spatial profile (with uncalibrated spatial dimension) and the pinpoint density is shown in Figure A2 for BD-7-PY-37, Site 2705 at 1 ns. This procedure yielded pinpoint density maps which closely matched the damage observed in the sample as a comparison of Figure A1-2 to Figures 12 and 13 of the text illustrates.
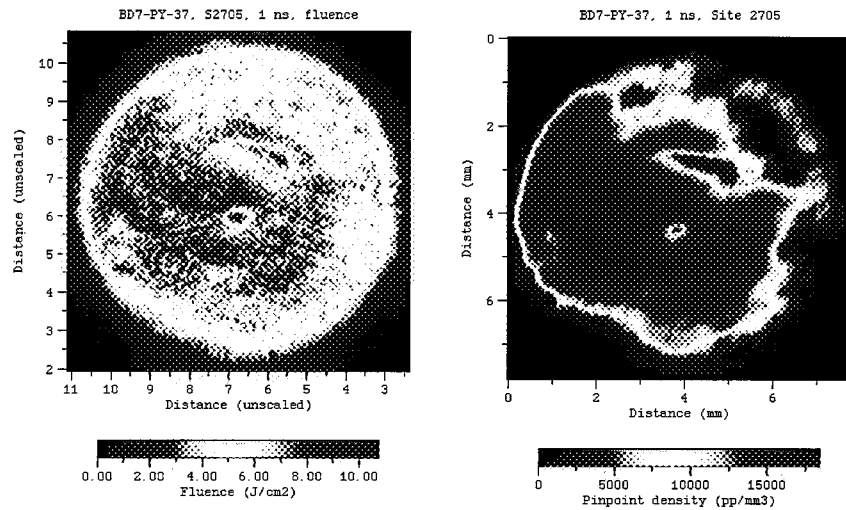

Figure A1-2. Comparison of pinpoint density (right) to spatial profile (left) for BD-7-PY-37, Site 2705 at 1 ns. The maximum fluence in the beam is on the order of 10 J/cm^2. The high density portions of the scatter map correspond well to the high fluence portion of the beam.